DAA/LANGLEY

IN-34
69606
CR

P.32

Semi-Annual Progress Report
NASA Grant NAG-1-507
MIT OSP No. 95315

Research in Computational Fluid Dynamics

Reporting Period
September 1, 1986 - February 28, 1987

Submitted to

Mr. Duane Melson
Technical Monitor
Mail Stop 159
NASA Langley Research Center
Hampton, Va. 23665-5225
(804) 865-2627

Submitted by
Professor Earll M. Murman
Principal Investigator
Department of Aeronautics and Astronautics
Massachusetts Institute of Technology
Cambridge, MA 02139

Submitted April 27, 1987

(NASA-CR-180542) RESEARCH IN COMPUTATIONAL FLUID DYNAMICS Semiannual Progress Report, 1 Sep. 1986 - 28 Feb. 1987 (Massachusetts Inst. of Tech.) 32 p Avail: NTIS HC A03/MF A01 CSCL 20D G3/34
N87-27128
Unclas
0069606

Report

The activities of this grant are divided into two tasks, each with a graduate student, a faculty advisor, and a separate topic.

For the first task, Mr. Mehtab Pervaiz is working with Professor Judson R. Baron on spatial and temporal adaptive algorithms for reacting flows. A paper was prepared for and presented at the First World Congress on Computational Mechanics held at University of Texas at Austin in September 1986. The attached copy of the paper summarizes the research in progress. Between September and February, interest has shifted to two dimensional flows.

For the second task, Mr. Steven Ruffin is working with Professor Earll M. Murman on hypersonic viscous calculations for delta wing geometries. The conical Navier-Stokes equations model has been selected in order to investigate the effects of viscous-inviscid interactions. The more complete three-dimensional model is beyond the available computing resources. The flux vector splitting method with van Leer's MUSCL differencing is being used. Both two and three stage Runge-Kutta time marching schemes have been investigated. A detailed von Neumann stability analysis has been performed for selecting the coefficients for each stage. Preliminary results have been computed for several conditions. Mr. Ruffin visited NASA Langley in January 1987 to work for a week with Dr. James Thomas on development of the numerical approach.

TEMPORAL AND SPATIAL ADAPTIVE ALGORITHM FOR REACTING FLOWS *

MEHTAB M. PERVAIZ

JUDSON R. BARON

COMPUTATIONAL FLUIDS DYNAMICS LABORATORY
DEPARTMENT OF AERONAUTICS AND ASTRONAUTICS
MASSACHUSETTS INSTITUTE OF TECHNOLOGY
CAMBRIDGE, MASSACHUSETTS 02139

* Presented at First World Congress on Computational Mechanics held at University of Texas at Austin, Sept. 1986.

---

1 Introduction

This paper discusses the numerical integration of quasi-one-dimensional unsteady flow problems which involve finite rate chemistry and are expressed in terms of conservative form Euler and species conservation equations.

The coupled behavior between fluid flow and finite rate chemistry can introduce appreciable stiffness into numerical integration schemes, which then involve prohibitively long computation times. The use of globally fine grid resolution to ensure the capture of local flow features can also result in lengthy runs. The aim of the present paper is to provide a description of a controlled grid resolution approach in both space and time, and to demonstrate its advantage in diminishing the stiffness constraint.

The use of uniform spatial and temporal grids demands some form of equilibrium limit modeling for extremely fast kinetics. However, the retention of a fine grid resolution when approaching that limit is required only for small portions of the overall space/time domain. Typically, fine *spatial* resolution is desired in those regions in which a shock or species concentration results in very rapid local changes; similarly high *temporal* resolution is needed where there are large non-equilibrium source terms which produce large temporal gradients. We discuss an adaptive technique which refines the spatial and/or temporal grid whenever preselected gradients exceed certain threshold levels. In general the resolved grid field is itself unsteady, and its rate of change may vary from large values for certain unsteady problems to zero for steady state solutions. For example, the adapted grid for a moving shock must track the discontinuity.

The present algorithm involves periodic examination of the evolving solution, detection of those regions in which large spatial non-uniformities exceed a threshold limit, and subsequent subdivision of the corresponding grids. Reverse embedding (collapse) to a coarser mesh is allowed up to the initial (coarsest) global grid. Consistent pre-embedding in accord with the initial flow field is appropriate.

For unsteady flow the temporal gradients must be monitored so as to maintain sufficiently small time-steps for adequate local resolution and stability. However, temporal adaptation does allow for spatial variation of the cell time-steps, without which a global minimum time-step would apply and could be extremely costly.

2 Governing Equations

The unsteady, conservation form, quasi-one-dimensional Euler equations, for a reacting gas may be represented by the vector equation

$$\frac{\partial U}{\partial t} + \frac{\partial F}{\partial x} = W \tag{1}$$

Here

$$U = \begin{pmatrix} \rho A \\ \rho A u \\ A\epsilon \\ \rho A Y_s \end{pmatrix}, \qquad F = \begin{pmatrix} \rho A u \\ A(\rho u^2 + p) \\ Au(\epsilon + p) \\ \rho A u Y_s \end{pmatrix}, \qquad W = \begin{pmatrix} 0 \\ p dA/dx \\ 0 \\ \dot{W}_s \end{pmatrix} \tag{2}$$

where ρ, u, ϵ, p and A are the density, velocity, total energy per unit volume, pressure and stream-tube area, respectively. Y_s denotes the mass fraction of the s^{th} species ($s = 1, \cdots, S$) and $\dot{W}_s$ is the associated chemical source term. The vectors U, F and W each have $3 + S$ components, however $\sum_{s=1}^{S} Y_s = 1$ so that only $S - 1$ species equations need to be considered. An equation of state for an ideal gas mixture is assumed

$$p = \rho \mathcal{R} T \sum_s Y_s / \hat{m}_s \tag{3}$$

Here $\hat{m}_s$ is the molecular mass of species s and $\mathcal{R}$ is the universal gas constant. The total energy is

$$\frac{\epsilon}{\rho} = \sum_s Y_s \{ H_{f_s} + \int_{T_{0_s}}^{T} C_{v_s} dT \} + \frac{u^2}{2} \tag{4}$$

where H_{f_s} is the heat of formation at reference temperature T_{0_s} and C_{v_s} is the constant volume specific heat, assumed to be constant for the adaptive examples to be shown.

For R reactions of the form

$$\sum_{s=1}^{S} \alpha_{sr} A_s \quad \rightleftharpoons \quad \sum_{s=1}^{S} \beta_{sr} A_s \ , \qquad r = 1, \cdots, R \tag{5}$$

stiffness arises from the source terms

$$\dot{W}_s = A \hat{m}_s \sum_{r=1}^{R} (\beta_{sr} - \alpha_{sr}) \left[\Omega_{fr} - \Omega_{br} \right] \tag{6}$$

in accord with differences in the Ω_l for forward, backward progress rates. For the *rth* reaction

$$\Omega_l = K_l \prod_{s=1}^{S} \left(\frac{\rho Y_s}{\hat{m}_s}\right)^{\sigma} \tag{7}$$

where $\sigma = \alpha_{sr}, \beta_{sr}$ for $l = fr, br$. The rate constants are assumed to be of the generalized Arrhenius form

$$K_l = A_l T^{\eta} \exp(-E_l/T) \tag{8}$$

3 Integration Scheme

The integration basis is a generalization of the second order accurate Lax-Wendroff finite volume scheme in Ref. [1]. Variables U, fluxes F and the source terms W are stored at the nodes. The generalization introduces non-uniform spatial grids and chemical source terms. Consider the cells B and C adjacent to node j (Fig. 1). The temporal change in state at node j is

$$\delta U_j \equiv U_j^{n+1} - U_j^n = \left.\frac{\partial U}{\partial t}\right|_j^n \Delta t + \frac{1}{2}\left.\frac{\partial^2 U}{\partial t^2}\right|_j^n \Delta t^2 + O(\Delta t^3) \tag{9}$$

or, using Eqs. (1),

$$\delta U_j = \{W - \frac{\partial F}{\partial x}\}\Delta t + \frac{\Delta t^2}{2}\left[W_U\{W - \frac{\partial F}{\partial x}\} - \frac{\partial}{\partial x}\left(F_U\{W - \frac{\partial F}{\partial x}\}\right)\right] \tag{10}$$

where, for example,

$$W_U = \left(\frac{\partial W}{\partial U}\right)_j^n \tag{11}$$

The flux balance for cell C, *e.g.*, yields the *cell change*

$$\Delta U_C = W_C^* \Delta t_C + (F_j - F_k)\,\frac{\Delta t_C}{\Delta x_C} \tag{12}$$

in which W_C^* may be modelled as an average

$$W_C^* = (W_j + W_k)\,/2 \tag{13}$$

Alternatively, for a more accurate contribution to node j use can be made of a ΔU_{jC} based on choosing $W_C^* = W_j$, in which case

$$\Delta U_{jC} = W_j \Delta t_C + (F_j - F_k)\,\frac{\Delta t_C}{\Delta x_C} \tag{14}$$

We shall use Eq. (12) for the determination of Δt and Eq. (14) for the integration scheme.

In terms of a non-uniform grid parameter

$$\epsilon_j = \frac{\Delta x_B - \Delta x_C}{\Delta x_B + \Delta x_C} \tag{15}$$

a second order accurate expression for the rate of change of a scalar variable ϕ is

$$\left.\frac{\partial \phi}{\partial x}\right|_j = \frac{1+\epsilon_j}{2\Delta x_C}(\phi_k - \phi_j) - \frac{1-\epsilon_j}{2\Delta x_B}(\phi_i - \phi_j) + O\left(\Delta x_B \Delta x_C\right) \tag{16}$$

Using this and Eq. (14) to discretize Eq. (10) the resulting overall change δU_j is comprised of contributions from cells B and C, *i.e.*,

$$\delta U_j = \delta U_{jB} + \delta U_{jC} \tag{17}$$

where

$$\begin{aligned} \delta U_{jB} &= \tfrac{1-\epsilon_j}{2}\left[\Delta U_{jB} + \tfrac{\Delta t_B}{\Delta x_B}\left(\Delta F_B + \tfrac{2\epsilon_j}{1-\epsilon_j}\Delta F_{jB} + \Psi_B\right) + \tfrac{\Delta t_B}{2}\Delta W_{jB}\right] \\ \delta U_{jC} &= \tfrac{1+\epsilon_j}{2}\left[\Delta U_{jC} - \tfrac{\Delta t_C}{\Delta x_C}\left(\Delta F_C - \tfrac{2\epsilon_j}{1+\epsilon_j}\Delta F_{jC} + \Psi_C\right) + \tfrac{\Delta t_C}{2}\Delta W_{jC}\right] \end{aligned} \tag{18}$$

Here, for example,

$$\Delta F_C = \left.\frac{\partial F}{\partial U}\right|_C \Delta U_C \quad , \qquad \Delta F_{jC} = \left.\frac{\partial F}{\partial U}\right|_j \Delta U_{jC} \tag{19}$$

An artificial viscosity contributes to the above two changes and is of the form

$$\Psi_C = (\sigma_j + \sigma_k)(U_j - U_k)/4 \tag{20}$$

The nodal viscosity coefficients are obtained from

$$\sigma_j = \sigma_{min} + \delta(\kappa_B + \kappa_C) \tag{21}$$

where, for example,

$$\kappa_C = \left|\frac{\rho_j - \rho_k}{\rho_j + \rho_k}\right| \tag{22}$$

The constant δ is chosen so that $\sigma_j \in [\sigma_{min}, \sigma_{max}]$, typically between 0.05 and 0.5.

4 Spatial Adaptation

For a system of K equations each and every state variable $U(k), k = 1, \cdots, K$, need not be considered to define the necessary spatial and temporal resolution. Pre-selected variables for such space and time resolution criterion are referred to here as *spacrit* and *tempcrit*, respectively. A typical choice for *spacrit* is density since it appears as a factor in each element of the state vector; furthermore, density differences are present for most flow fields including contact discontinuities, and have been shown to be the an appropriate choice for a class of problems by numerical experimentation, Ref. [2].

When carrying out computations a distinction must be made between interests in steady and unsteady situations. Steady state problems may involve multiple grids and other acceleration techniques, whereas unsteady flows may not involve such procedures. Spatial adaptation can be done occasionally in steady flows and the number of such operations equals those of the spatially embedded levels desired; however for unsteady flows the spatial adaptation may have to be applied after each *time-stride.* The latter is defined as the time interval between the constant time surfaces for the entire spatiotemporal domain. It is more appropriate to use *local time-stepping* than temporal adaptation for steady flows.

The choice of initial grid conditions is of some importance for unsteady flow. If large spatial gradients are present in the initial flow field and the spatial grid is coarse in their vicinity, the initial integrated solution will be degraded and will propagate as such to other spatial locations at later time levels. For that reason all initial flow fields are examined for first differences of *spacrit*, and wherever the critical limit is exceeded the grid is *pre-embedded, i.e.,* some spatial resolution is added at appropriate locations before integrating the equations. For example a shock tube problem suggests that finer cells be inserted near the contact discontinuity surface.

Upon initiating the integration scheme, the evolving solution is periodically reexamined for regions of relatively large gradients of *spacrit*; if the threshold limit is exceeded the grid is divided locally . Alternatively, when associated gradients diminish on a previously refined grid, and become less than another critical limit, those contiguous grids may be collapsed while making certain that the cells to be merged are those from the same parent cell. The initial (coarse) global grid is kept stagnant by insisting that the coarsest cells (spatial level zero) be never merged to a coarser state, no matter how smooth the evolving solution proves to be. The choice of spatial threshold limits is similar to that for perfect gases [2,3].

The *spatial interfaces* are defined to be the nodes which are at the boundary of widely disparate cell sizes ($|\epsilon| \geq \frac{1}{3}$). A special formulation of artificial viscosity is used at the spatial interface for the steady flow situations due to the coupling with multiple grids. When integrating the coarse cells adjacent to the spatial interface, the artificial viscosity coefficient is obtained by using Eq. (21) in the usual manner; however, for the neighbouring fine cell this coefficient is doubled when applying the contribution to the common node for steady flow situations. Such a special formulation is unnecessary for unsteady cases since multiple grids are not used.

Currently there are two major approaches for spatial adaptation procedures: grid point redistribution (or moving elements) and locally embedded grids. The current paper belongs to the latter class. A study that is typical among numereous grid point redistribution schemes is reference [4] while a local spatial embedding example is [5].

5 Temporal Adaptation

The temporal and spatial adaptation procedures are inherently different and can be applied separately. The spatial adaptation process is carried out at the current time level at all spatial locations and may not be done as many number of times as the temporal adaptation. The frequency of spatial adaptation depends upon the time rate of change of the flow feature being resolved. The temporal adaptation, on the other hand, is repeated after each *time-stride* at all spatial locations and must anticipate the subsequent changes in the the flow field. The three steps for completing a temporal grid adjustment are :

1. a determination of the allowable Δt for each cell
2. reassignment of consistent Δt distributions such that adjacent cells differ by a factor of 2 at most
3. determination of a proper integration sequence over the cell domain.

The first order change with time from Eq. (12) is given for cell C by

$$\Delta U_C = \Delta t_C \left(W_C^* + \frac{F_w - F_e}{\Delta x_C} \right) \approx \frac{\partial U}{\partial t} \Delta t_C \tag{23}$$

in terms of the west, east fluxes F_w, F_e; and is subject to the usual CFL restriction

$$\Delta t_{stb} \leq \frac{\Delta x_C}{|u| + a_f} \tag{24}$$

a_f being the local frozen speed of sound. In addition, the resolution requirement, Δt_{res}, follows from a threshold criterion which is based on the maximum allowable change, $\Delta U_{C_{max}}$, for the *tempcrit* variable; *i.e.*

$$|\Delta U_C| \leq \Delta U_{C_{max}} = |\epsilon_1 U_C + \epsilon_0| \tag{25}$$

where the ϵ_i are small positive numbers. Effectively, the change is limited to a fraction of the state value excepting for vanishingly small levels. Unlike the choice of *spacrit* that for *tempcrit* is not obvious here. It should, however, correspond to the maximum rate of change of a species. The fact that exchange reactions are generally faster than the dissociation reactions can be important in selecting *tempcrit.* Comparing Eqs. (23) and (25)

$$\Delta t_{res} = \frac{|\epsilon_1 U_C + \epsilon_0| \Delta x_C}{W_C \Delta x_C + (F_w - F_e)} \tag{26}$$

The resolution requirement, Δt_{res}, may or may not exceed the stability requirement, Δt_{stb}, and the actual time-step is

$$\Delta t = \min\{\Delta t_{res}, \Delta t_{stb}\} \tag{27}$$

Note that for non-reacting uniform flow $\Delta t_{res} \longrightarrow \infty$ and the stability requirement is governing. On the other hand, large W_C implies $\Delta t_{res} \ll \Delta t_{stb}$ and the expected problem of *stiffness.* If time accurate descriptions are sought, a criterion such as Eq. (26) is required for both explicit and implicit integration schemes. Equation (26) also satisfies the stability restriction imposed on the explicit schemes due to the chemical source terms.

Based on the global minimum and maximum Δt constraints over the spatial domain, a ***current allowable temporal level*** m for the cells is assigned such that

$$2^m \leq \min\{\frac{\Delta t_{max}}{\Delta t_{min}}, 2^M\} < 2^{m+1} \tag{28}$$

Here m is equal to or less than a pre-selected maximum level, M, and is chosen to avoid what will be referred to as ***temporal level stiffness.*** A flow feature generally implies an associated characteristic speed, *e.g.* that for a shock or reaction, and the spatially embedded region must be sufficiently large to ensure that the feature will remain within the embedded region during the subsequent ***time-stride.*** The ***size of a time-stride*** depends upon the value of M. An excessively large size makes possible a departure of the feature from the spatially embedded region. Hence the embedded portion must be enlarged for large time-strides. Though temporal embedding involving large time-strides helps to reduce CPU time, the increased number of nodes can be expensive and a balance between the two competing effects is necessary. This represents one facet of ***temporal level stiffness.***

The actual time-steps are re-assigned for a given cell C, according to

$$\Delta t_C^{new} = 2^n \Delta t_{min} \tag{29}$$

where level $n \leq m$ is given by

$$2^n \leq \min\{\frac{\Delta t_C}{\Delta t_{min}}, 2^m\} < 2^{n+1} \tag{30}$$

The total number of time-strides for level n cells is 2^{m-n}. Figure 2 shows an example of cell time-steps before and after reassignment. The numbers in part *(a)* indicate the initial time-steps in terms of Δt_{min}; part *(b)* shows the adjusted time-steps for $m = 2$. The ***temporal interface*** will be referred to as ***nodit*** (Node Of DIfferent Time-steps) in the following.

The order in which the integration over the cells takes place is of special importance. For example, if the level 0 cells labelled A_i in Fig. 2b are integrated four times consecutively use is made only of information based on the two nodes d and e. This is correct for A_1, but for A_4 additional account must somehow be taken of the nearby nodes. If for seven integration passes, we integrate level 0 cells on pass 1, level 1 cells on pass 2, level 0 cells on pass 3, level 2 cells on pass 4 and so on as indicated by the numbers in Fig. 2b, by the time A_4 will be integrated the nodes d and e will have accumulated effects from nodes a through g, provided that after each integration pass the cells at a particular level have been updated and the flux, source terms and Jacobians recomputed. This represents a second facet of ***temporal level stiffness.***

The total number of integration passes is

$$P_T = 2^{m+1} - 1 \tag{31}$$

A complete cycle of P_T integration passes will be referred to as a ***time-stride***, and m its ***size.*** On pass $P \in [1, P_T]$ we integrate level n cells if

$$\frac{P - 2^n}{2^{n+1}} = integer \tag{32}$$

No special formulation is needed at the nodits (which are not necessarily spatial interfaces) and in order to render the actual spatial location of any temporal level cell irrelevant, the data base must be constructed so as to store the cells with same temporal level together. There is no such restriction for the spatial adaptation pointers.

Since both nodes of a cell are updated after each integration pass, and the flux, etc., are recomputed, the state at a nodit *during* a time-stride is not time-accurate; however, on completion of a time-stride the state is temporally correct. As an example consider the situation depicted in Fig. 3 where $\Delta t_C = 2\Delta t_B$. On the first pass over cell B, the contribution to node j, δU_{jB}, is computed from Eq. (18) based on the flux values at time level (n),so that a new state $(*)$ at node j can be defined as

$$U_j^* = U_j^n + \delta U_{jB}^{n,n} \tag{33}$$

The supercript (n, n) indicates that both nodes i and j of cell B use values at time level (n). The state $(n+1)$ at node i is defined in the usual manner

$$U_i^{n+1} = U_i^n + \delta U_{iA}^{n,n} + \delta U_{iB}^{n,n} \tag{34}$$

On the second pass cell C is integrated using values at the time level $(*)$ for node j and time level (n) for node k and a new state $(\dagger)$ is defined at node j as

$$U_j^\dagger = U_j^* + \delta U_{jC}^{*,n} \tag{35}$$

where, $\delta U_{jC}^{*,n}$ is evaluated from Eq. (18), making use of, for example,

$$\Delta U_{jC}^{*,n} = W_j^* \Delta t_C + (F_j^* - F_k^n)\frac{\Delta t_C}{\Delta x_C} \tag{36}$$

Finally, on the third pass cell B is integrated again using values at time level $(n+1)$ for node i and values at level $(\dagger)$ for node j. The result is

$$U_j^{n+2} = U_j^\dagger + \delta U_{jB}^{n+1,\dagger} \tag{37}$$

6 Results

Three examples have been considered to illustrate the technique: a streamtube flow and shock tube, each with a single dissociating gas, and a multiple reaction flow for a diverging channel. For the first of these a Lighthill ideal dissociating gas [6], $M_2 \rightleftharpoons 2M$, was assumed to be flowing through a converging-diverging streamtube with an area distribution $A = 1 + 0.5x^2$. The nonequilibrium source term may be written as

$$\dot{W}_M = \Phi T^\eta \rho \left[(1 - Y_M) e^{-\theta_D/T} - \frac{\rho}{\rho_D} Y_M^2 \right] \tag{38}$$

with the non-dimensional reaction parameter given by

$$\Phi = \frac{C_f T_r^\eta \rho_r L_r}{\hat{m}_M \sqrt{p_r/\rho_r}} \tag{39}$$

where C_f, η, θ_D and ρ_D are constants and subscript r denotes reference quantities. The rate parameter Φ varies from zero for frozen flow, to infinity for equilibrium flow.

An initial validation of the code consisted of shock free flow examples and comparison of results with [7] for several values of Φ. Figures 4 and 5 show results obtained with *local time-stepping* and a uniform grid; specifically the degree of dissociation and temperature distributions appear on a plot folded about the minimum area section such that the upper curves correspond to the subsonic upstream region. The *freezing* phenomenon is evident in the supersonic regions for intermediate Φ. The agreement with [7] was very good.

Figure 6 shows a real flow through the same parabolic nozzle for $\Phi = 10^4$ but with a back pressure ratio $p_b/p_r = 0.92$, so that a normal shock would be stationed at $x = 0.5$ for a frozen flow situation. Two levels of spatial embedding and local time-stepping were used for the adapted case. The results are shown corresponding to coarse, embedded and fine grids, with relative computing times 10.1 (fine/coarse) and 1.4 (adapted/coarse); the vertical scale corresponds to the coarse grid and the other two curves are displaced by the indicated offset. The embedded and fine grid solutions agree very well whereas the shock location is displaced and spread out for the coarse grid. Shown in Fig. 7 is the final grid and degree of dissocation for adapted and coarse grid cases, and indicates that the coarse grid solution predicts a different chemistry aft of the normal shock.

A second example was the shock tube flow for frozen and reacting cases, ($\Phi = 0, 10^4$). The initial conditions across the contact surface were $p_2/p_1 = 0.2$, $T_2/T_1 = 1.0$. Three levels of both spatial and temporal adaptations were introduced and the results shown correspond to $t = 0.6$. Figure 8 shows the progression of grids as time increases for the frozen case, whereas Fig. 9 shows the evolving temporal grid near time levels, $t = 0$ and $t = 0.2$.

Table 1: Comparison of CPU time for shock tube

	$\Phi = 0$	10^4	10^5
Coarse	1.00	1.21	1.89
Adapted	6.54	8.77	14.40
Fine	49.95	65.38	110.81

Figure 10 indicates the computational results for $\Phi = 10^4$ at the final time for coarse, adapted and fine grids and Fig. 11 indicates the evolution of density on the adapted grid. We again note that the coarse grid solutions are poorer than the fine or adapted grid solutions. Although results corresponding to $\Phi = 0, 10^5$ are not shown here, their CPU time comparisons are indicated in Table 1.

As a final example, multiple reactions were considered for the model in [8]. The reactions correspond to hydrogen combustion in air and are given by

$$\begin{array}{lclcl} H_2 & + & O_2 & \rightleftharpoons & 2OH \\ H_2 & + & 2OH & \rightleftharpoons & 2H_2O \end{array} \tag{40}$$

The forward rate constants (Eq. 8) are

$$\begin{array}{lcl} A_1 & = & (\frac{31.433}{\phi} \quad -8.917\phi \quad -28.95 \quad) \times 10^{44} \quad m^3/(kmole.s) \\ A_2 & = & (\frac{1.333}{\phi} \quad -0.833\phi \quad -2.00 \quad) \times 10^{58} \quad m^6/(kmole^2.s) \end{array}$$

$$\begin{array}{lcllcl} \eta_1 & = & -10 & \eta_2 & = & -13 \\ E_1 & = & 2448.4\ K & E_2 & = & 18940.6\ K \end{array}$$

where ϕ is the equivalence ratio. Backward rate constants were formed by using the equilibrium constants [9]

$$K_{e_1} = 26.164 e^{-8992/T}$$

$$K_{e_2} = 2.682 \times 10^{-9} T e^{+69415/T} \quad m^3/kmole$$

The streamtube area distribution is

$$\frac{A}{A_{min}} = \left[1 + \sin(\frac{\pi x}{4})\right]^2 \tag{41}$$

For this case use was made of two levels of spatial and ten levels of temporal embedding. The calculations were carried out to steady state (rms error of mass-fraction of $H_2 < 10^{-8}$) and took 4259*s* on a Microvax-II. For a *source implicit* scheme in [9] the same flow took 2524*s* on a CYBER-175 to converge. The comparative fine grid solution took three orders of magnitude longer. The results are shown in Figures 12 through 14 and proved to be in very good agreement with those of [9].

7 Discussion

A strategy has been developed for automatic spatial and temporal grid embedding for a quasi-one-dimensional, inviscid reacting flow. The spatial resolution was added prior to the execution of each temporal cycle (time-stride), was based on first differences of the density field, and avoided *spatial grid stiffness* by limiting the non-uniformity parameter to 2:1 grid ratios for any adjacent cells. The procedure allowed for both refinement of and return to coarser grids, within some specified coarsest global spatial grid. The temporal adaptation allowed for a factor of two or more difference in local time-steps for contiguous cells. The larger the global disparity of the cell time-steps the more effective is the temporal adaptation; as is true for spatial adaptation.

The finite volume, node based, scheme permits independent integration for each cell but requires increased artificial dissipation for finer cells at the spatial interfaces when multiple grids are used for steady state situations. The scheme also allows for separate pointer systems for spatial and temporal adaptation procedures.

The spatial data base tracks the spatial level, parent cell, and the surrounding nodes of each cell in the domain. Similarly, information about cells adjacent to each node must be known as well as that for special nodes such as the boundary and spatial interfaces. The temporal data base tracks the number of cells and the sequence of integration during each time-stride. This pointer system must be updated after each time-stride for assignments of time-steps, determination of the cell temporal level and its allocation into a cluster at the same level, determination of nodits, and constraining of time-steps across them (allowing only factors of two). Some of this represents an overhead but when compared to the gain achieved in efficiency proves to be well worth doing. Depending upon the problem, the spatial data base updating may not be required as frequently as the temporal data base. For steady state problems the number of changes in the spatial pointer system equal the number of spatially embedded levels desired and the adaptation can be performed at either specified iteration intervals or at any specified residual level. Similarly, for unsteady problems in which the characteristic feature speeds are relatively small the adjustments to the spatial pointer system are infrequent. However, when high feature speeds arise, either the time-stride size must be kept small or the spatially embedded clusters enlarged, so that the features do not move out of their respective clusters during a given time-stride. Furthermore the actual cell time-steps may change during a time-stride and hence the nodits might have to be moved to regions involving relatively less gradients. The process of enlarging spatially embedded clusters and translation of nodits can become computationally expensive; a balance is required between the competing effects of temporal level stiffness and temporal adaptation. The enlarging of the spatially embedded grids is accomplished by first determining the contiguous clusters of the refined cells and then refining those coarse cells which are outside and adjacent to be identical in level to those just inside the boundary, and repeating this a specified number of times. The translation of nodits similarly determines the nodits of clusters for contiguous cells with the same temporal level, and then halves the time-steps of the neighbouring cells with the larger time-step, repeating a specified number of times.

For all sample cases the numerical solutions with adaptation procedure were comparable in accuracy to globally fine grid solutions, and are in good agreement with previous works. Since the savings in CPU time are substantial for this quasi-one-dimensional study, it does appear promising to introduce temporal adaptation concurrently with spatial adaptation for multidimensional, unsteady reacting flow fields.

Acknowledgement

This work was supported by NASA under Grant NAG-1-507, technical monitor: Dr. James C. Townsend.

References

[1] Ni, Ron-Ho, "A Multigrid Scheme for Solving the Euler Equations", AIAA J, Vol. 20, No. 11, Nov. 1982, pp. 1565-1571.

[2] Dannenhoffer, J. F. and Baron, J. R., "Adaptive Procedure for Steady State Solutions of Hyperbolic Equations", AIAA Paper No. 84-0005, Jan. 1984.

[3] Dannenhoffer, J. F. and Baron, J. R., "Robust Grid Adaptation for Complex Transonic Flows", AIAA Paper No. 86-0495, Jan. 1986.

[4] Miller, K. and Miller, R. N., "Moving Finite Elements", SIAM J. Numer. Anal., Vol. 18, No. 6, Dec. 1981, pp. 1019-1032.

[5] Babuška, I. and Rheinboldt, W. C., "Error Estimates for Adaptive Finite Element Computations", SIAM J. Numer. Anal., Vol. 15, No. 4, Aug. 1978, pp. 736-754.

[6] Lighthill, M. J., "Dynamics of a Dissociating Gas", J. Fluid Mech., Vol. 2, No. 1, 1957, pp. 1-32.

[7] Bray, K. N. C., "Chemical and Vibrational Nonequilibrium in Nozzle Flows", "Nonequilibrium Flows", Editor P. P. Wegener, Vol. II, 1970, Marcel Dekker, Inc., pp. 59-157.

[8] Rogers, R. C. and Chinitz, W., "Using a Global Hydrogen-Air Combustion Model in Turbulent Reacting Flow Calculations", AIAA J, Vol. 21, No. 4, Nov. 1983, pp. 586-592.

[9] Drummond, J. P., Hussaini, M. Y. and Zang, T. A., "Spectral Methods for Modelling Supersonic Chemically Reacting Flow Fields", AIAA J, Vol. 24, No. 9, Sept. 1986, pp. 1461-1467.

LIST OF FIGURES

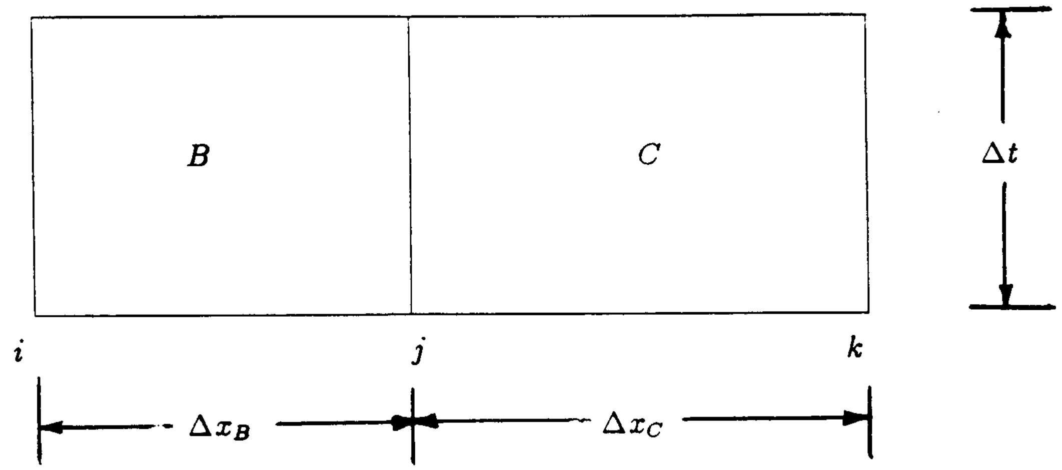
B
C
Δt
i
j
k
Δx_B
Δx_C

(a)

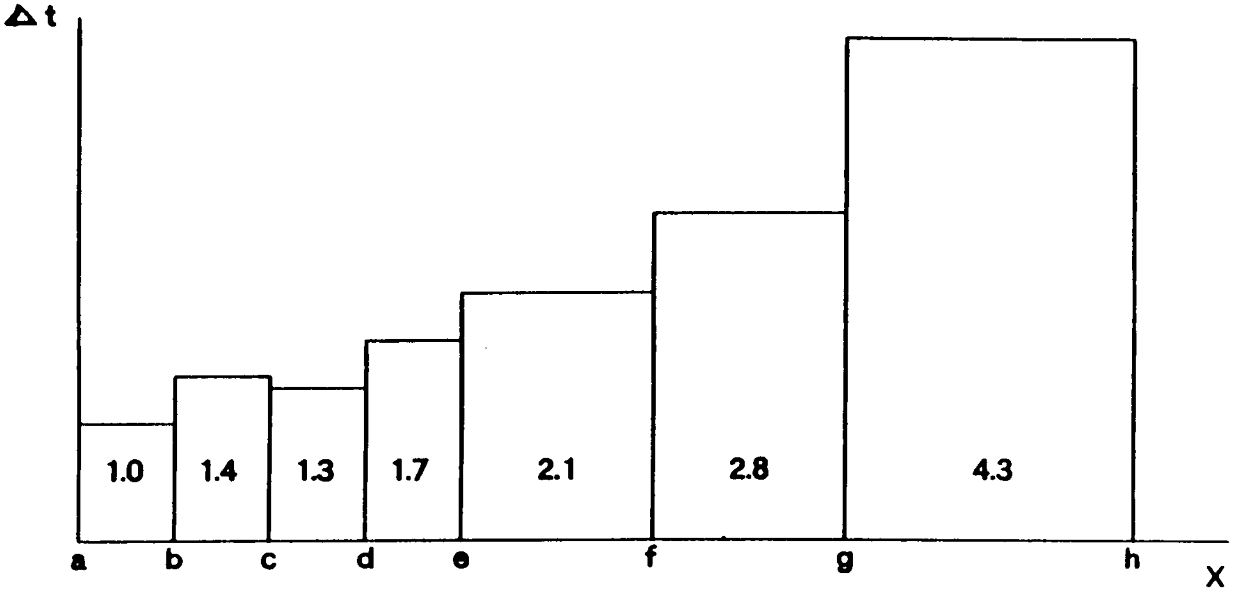
Δ t
1.0
1.4
1.3
1.7
2.1
2.8
4.3
a
b
c
d
e
f
g
h
X

(b)

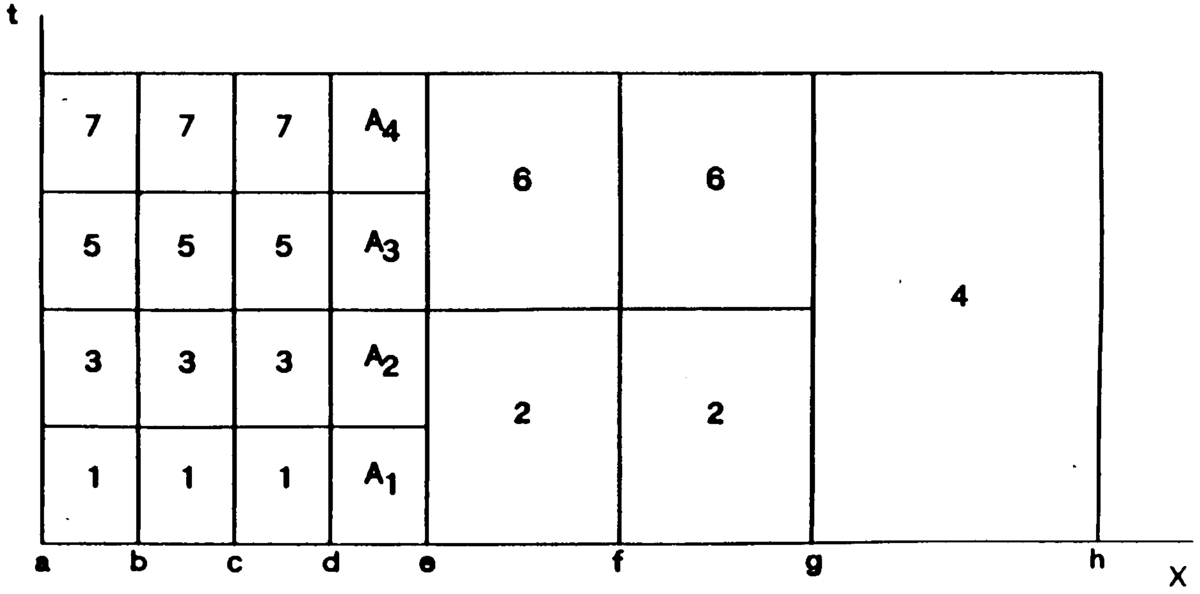
t
7
7
7
A4
5
5
5
A3
3
3
3
A2
1
1
1
A1
6
6
2
2
4
a
b
c
d
e
f
g
h
X

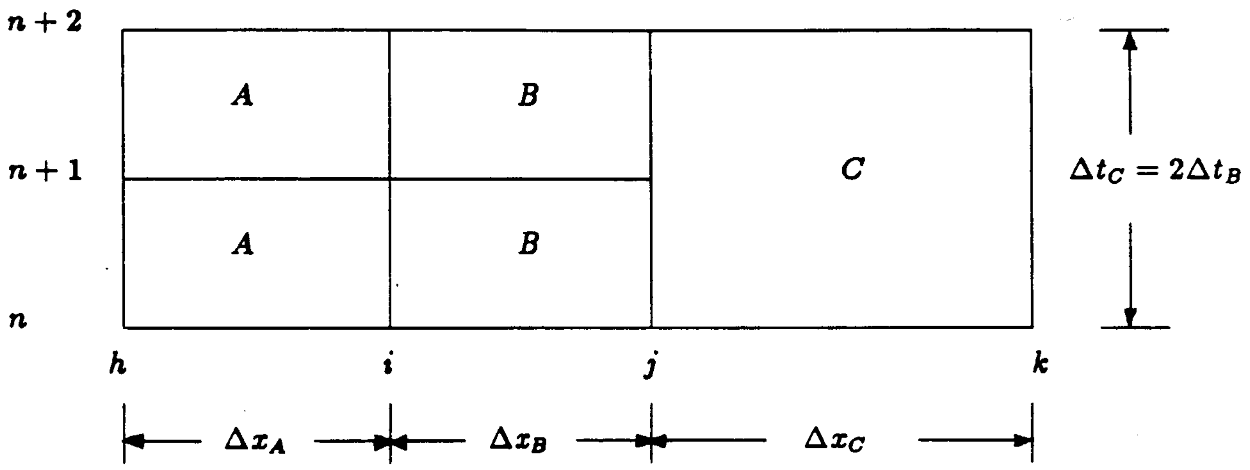
n + 2
n + 1
n
A
B
A
B
C
h
i
j
k
Δx_A
Δx_B
Δx_C
$\Delta t_C = 2\Delta t_B$

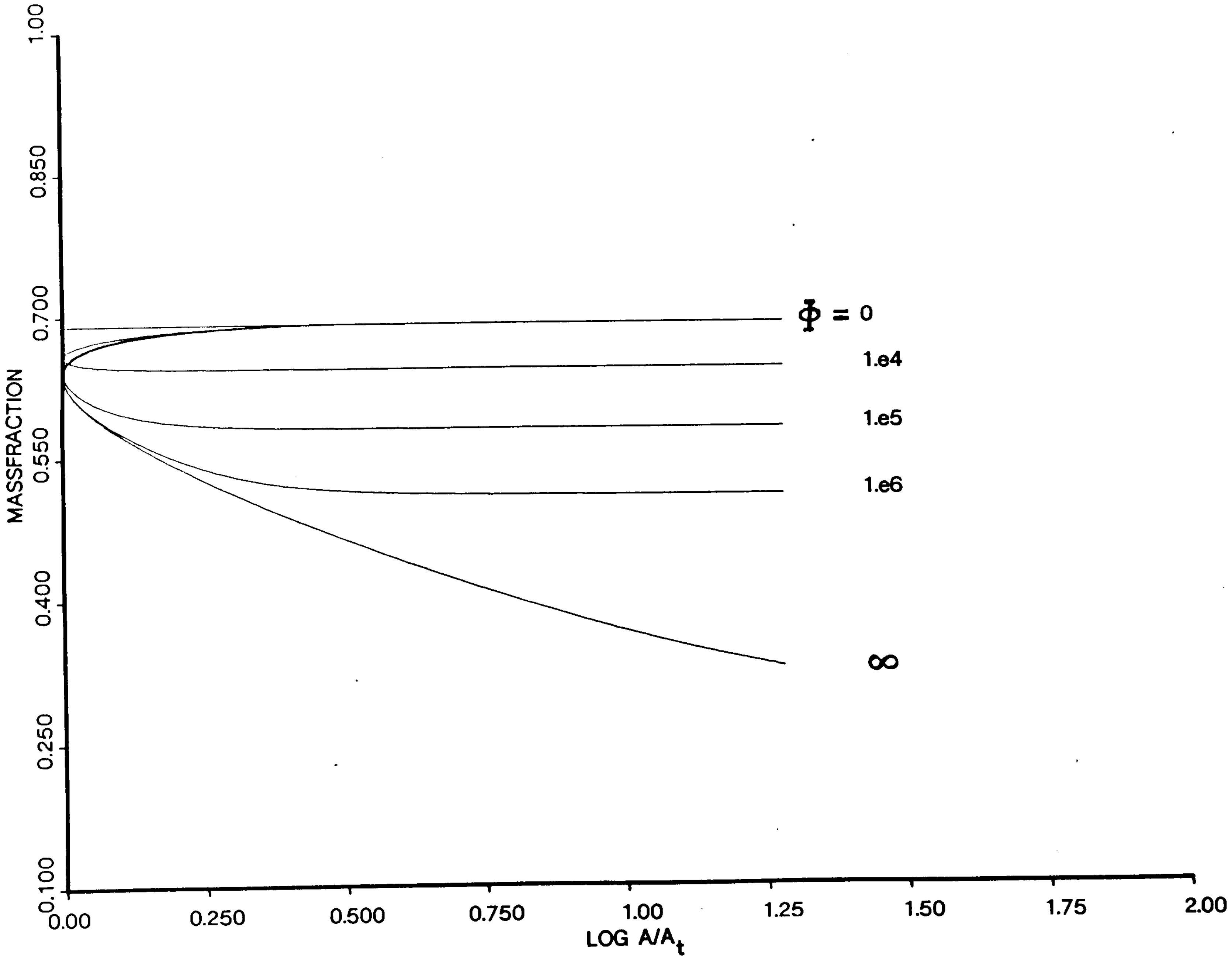
1.00
0.850
0.700
0.550
0.400
0.250
0.100
MASSFRACTION
0.00
0.250
0.500
0.750
1.00
1.25
1.50
1.75
2.00
LOG A/A$_t$
Φ = 0
1.e4
1.e5
1.e6
∞

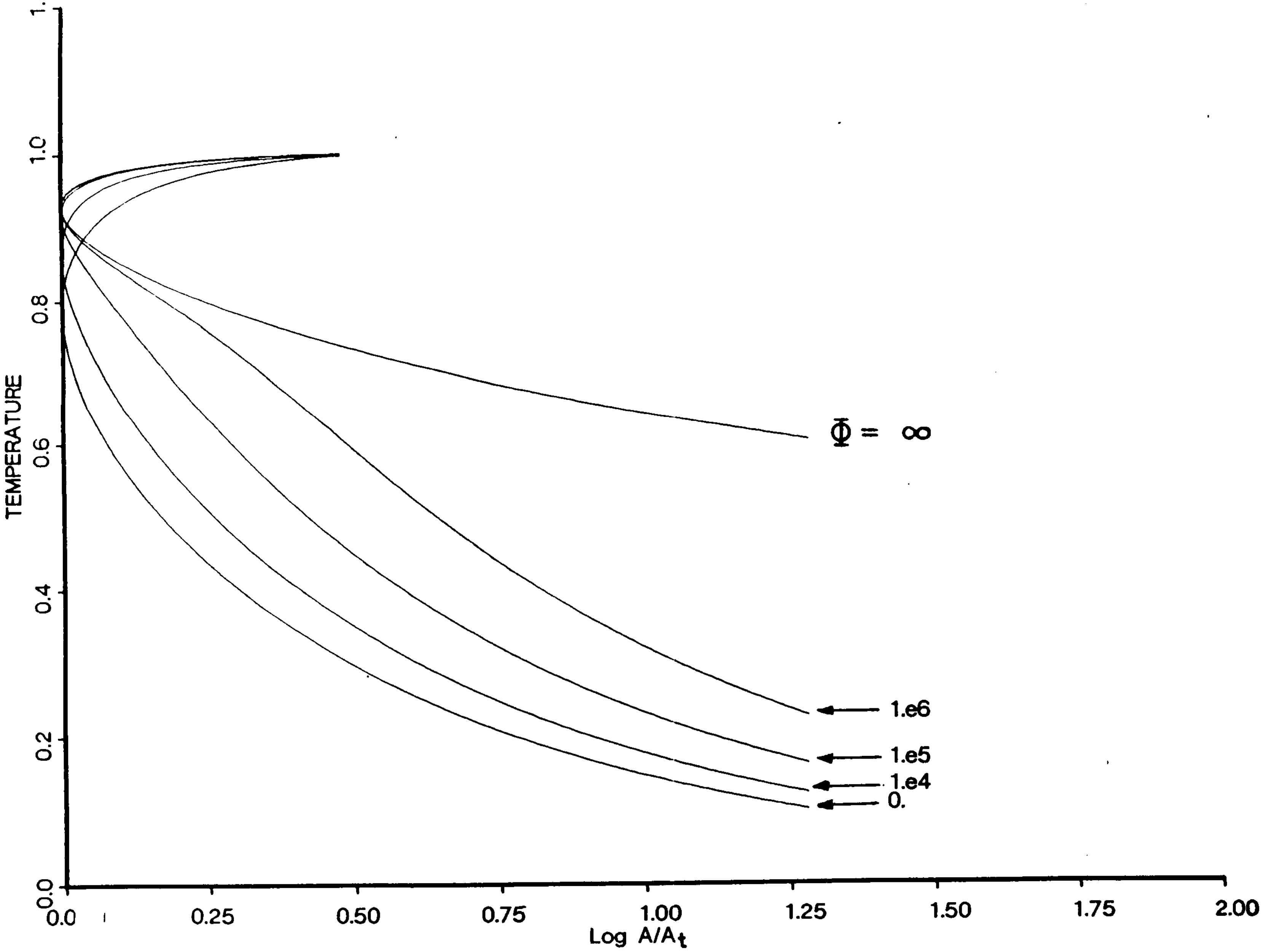
TEMPERATURE
0.0
0.2
0.4
0.6
0.8
1.0
1.2
0.0
0.25
0.50
0.75
1.00
1.25
1.50
1.75
2.00
Log A/A_t
$\Phi = \infty$
1.e6
1.e5
1.e4
0.

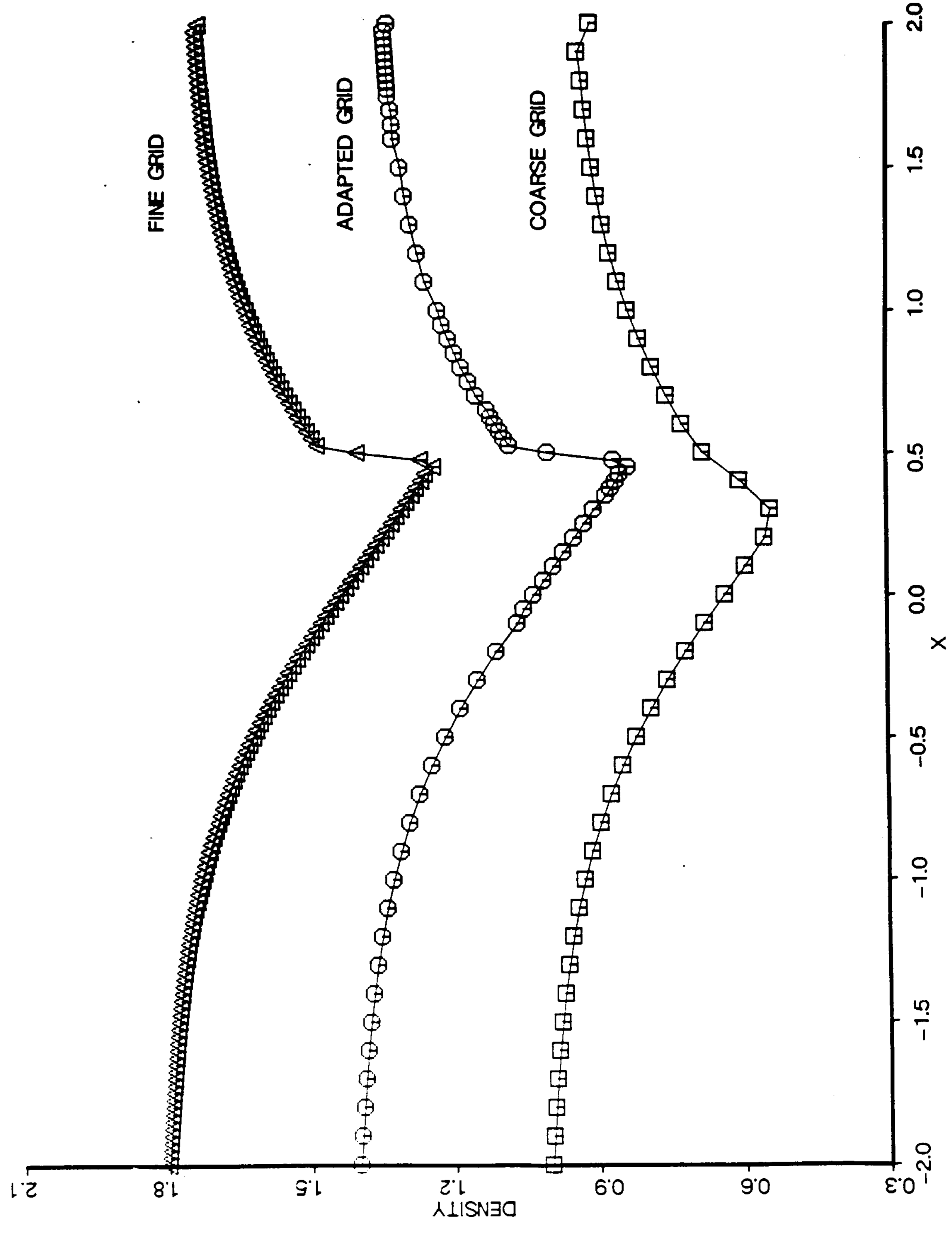
FINE GRID
ADAPTED GRID
COARSE GRID
DENSITY
X
0.3
0.6
0.9
1.2
1.5
1.8
2.1
-2.0
-1.5
-1.0
-0.5
0.0
0.5
1.0
1.5
2.0

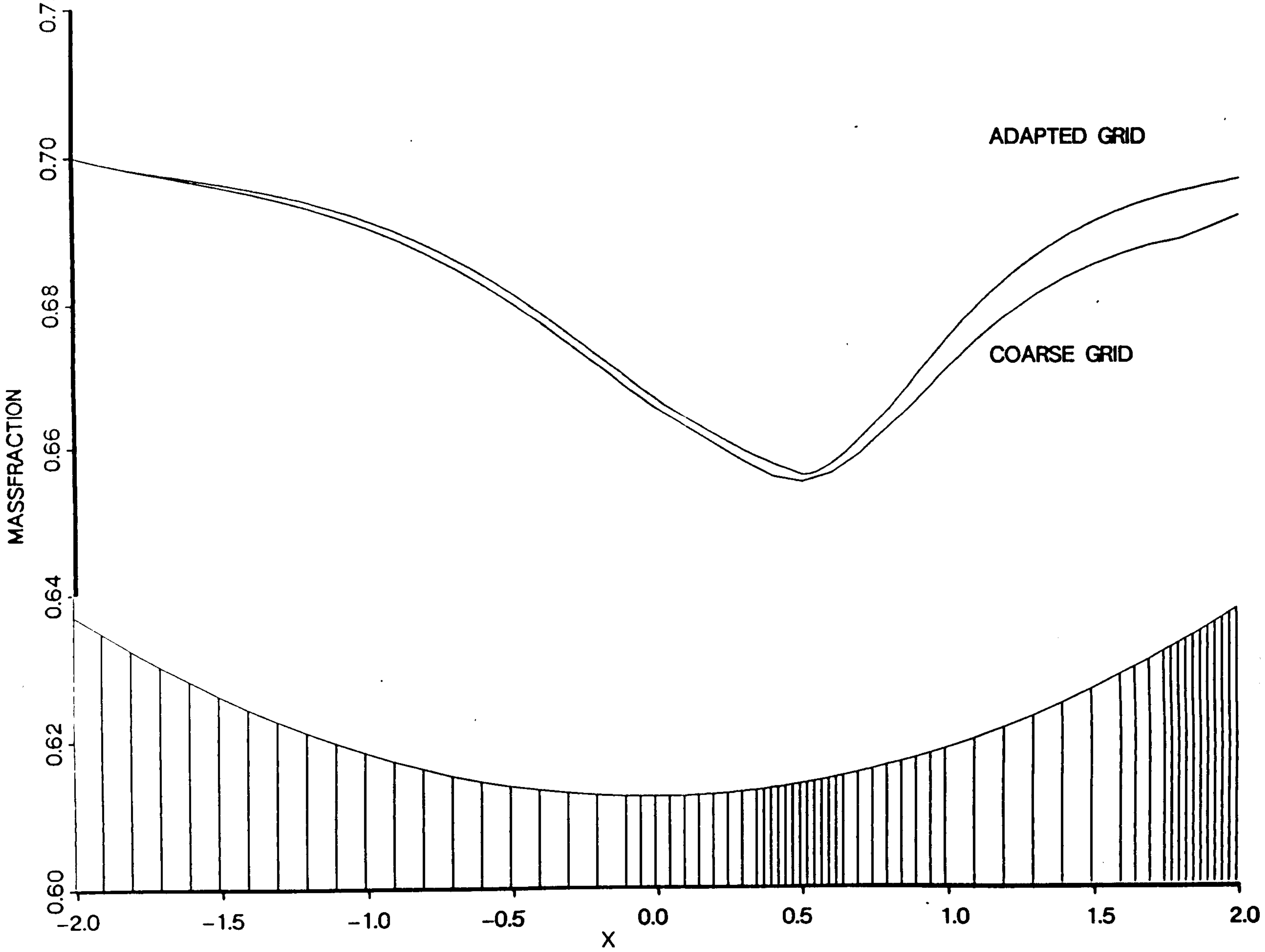
ADAPTED GRID
COARSE GRID
MASSFRACTION
0.72
0.70
0.68
0.66
0.64
0.62
0.60
X
-2.0
-1.5
-1.0
-0.5
0.0
0.5
1.0
1.5
2.0

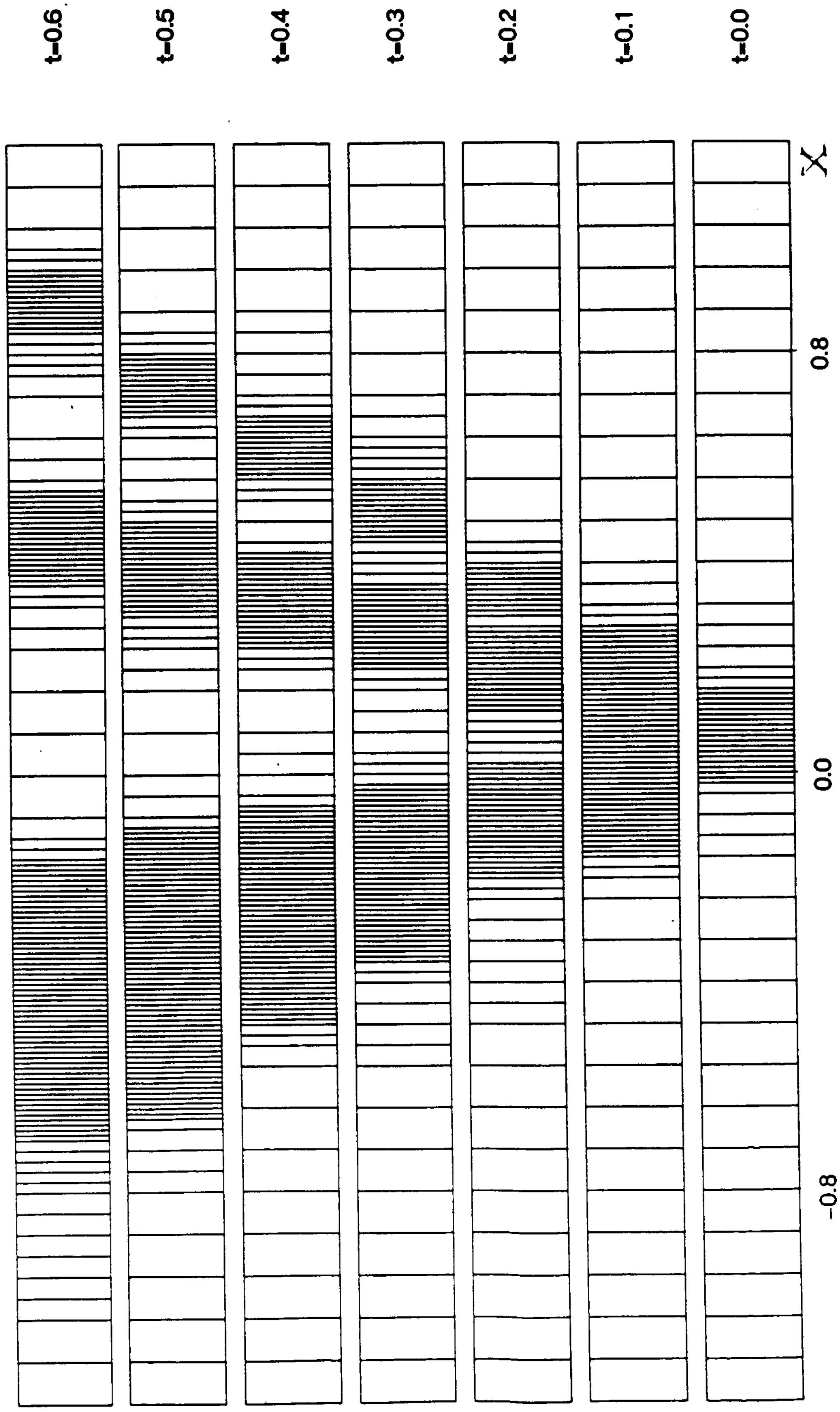
t=0.6
t=0.5
t=0.4
t=0.3
t=0.2
t=0.1
t=0.0
X
0.8
0.0
−0.8

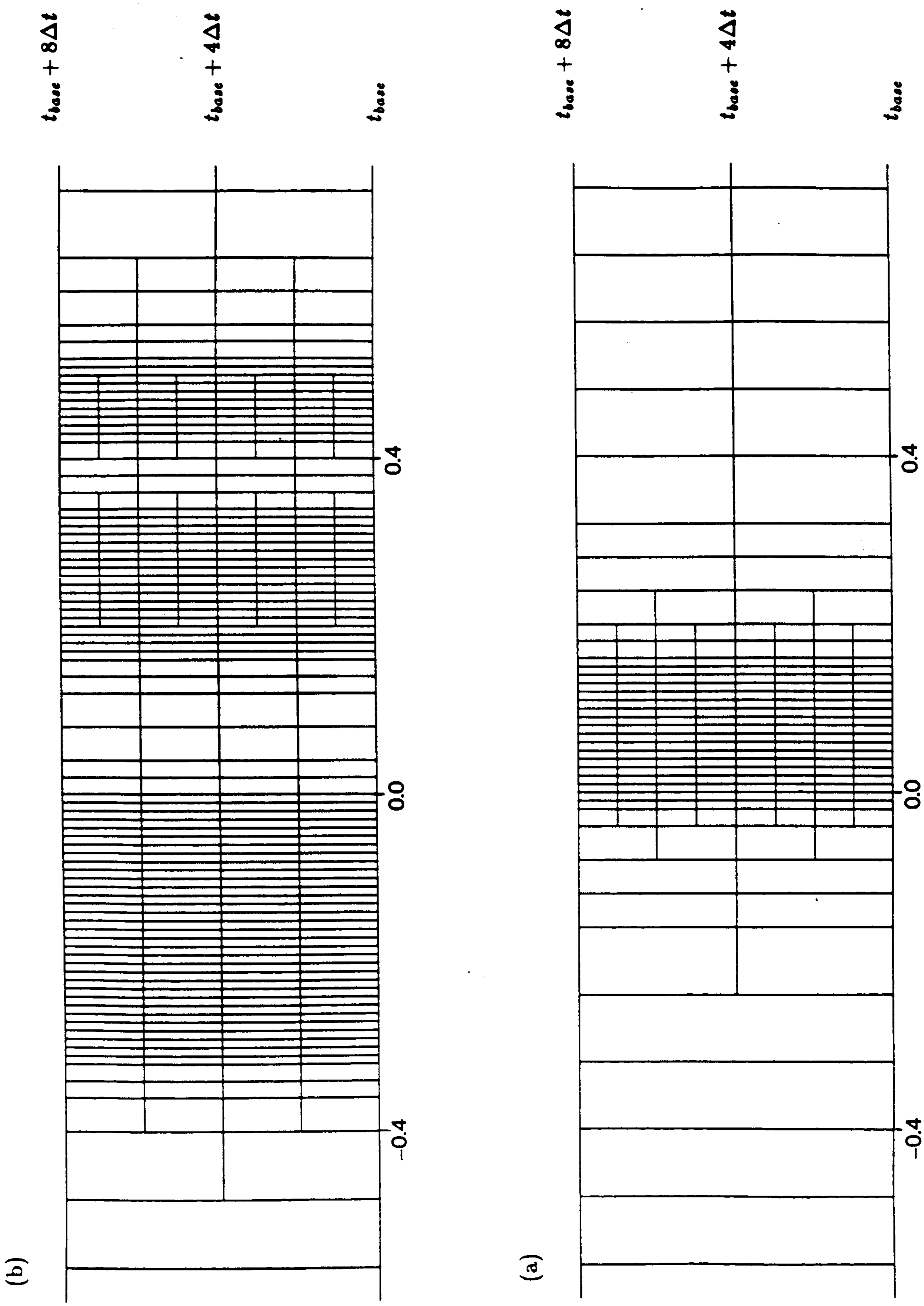
(a)
(b)
$t_{base} + 8\Delta t$
$t_{base} + 4\Delta t$
t_{base}
-0.4
0.0
0.4

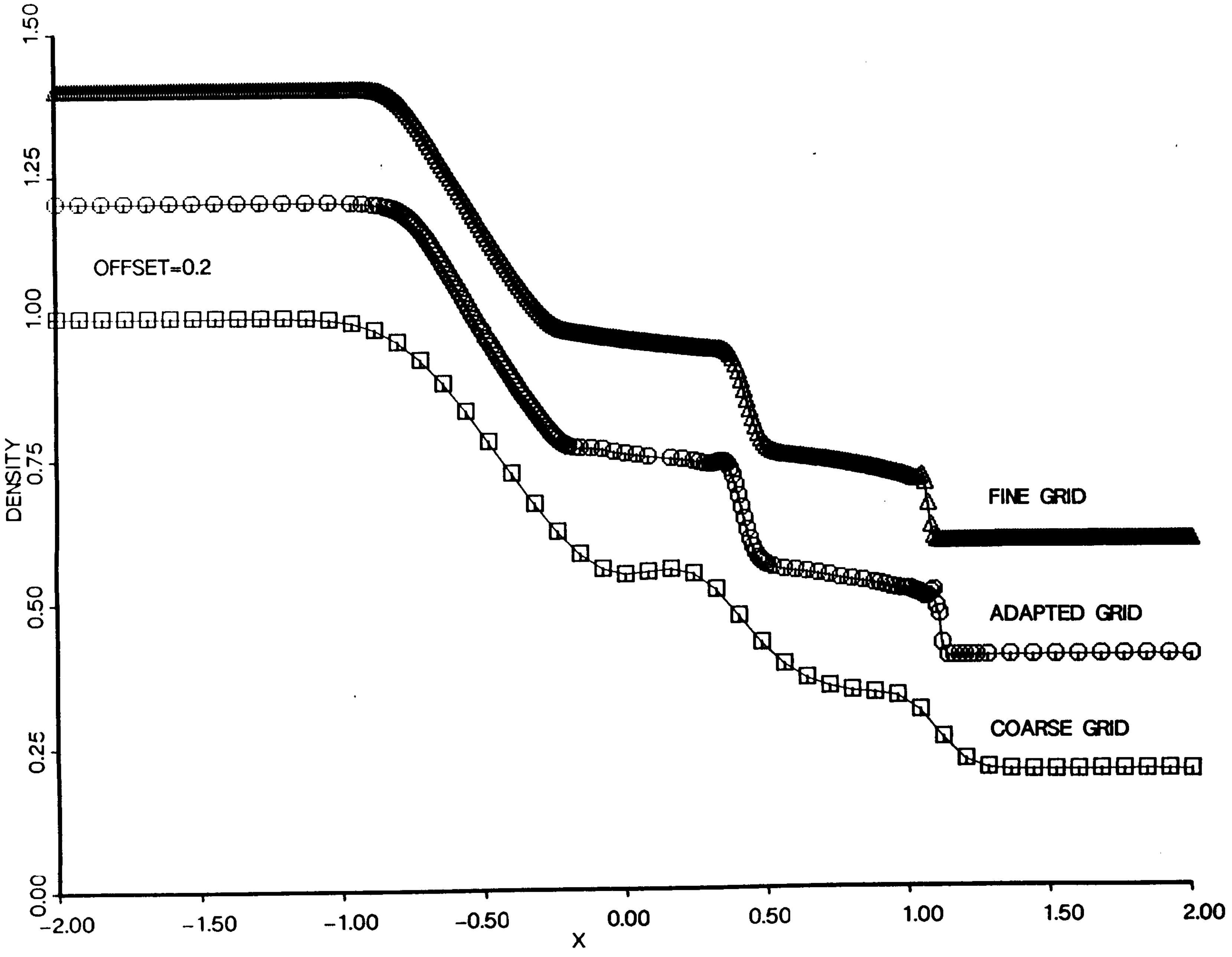
1.50
1.25
1.00
0.75
0.50
0.25
0.00
DENSITY
OFFSET=0.2
FINE GRID
ADAPTED GRID
COARSE GRID
-2.00
-1.50
-1.00
-0.50
0.00
0.50
1.00
1.50
2.00
X

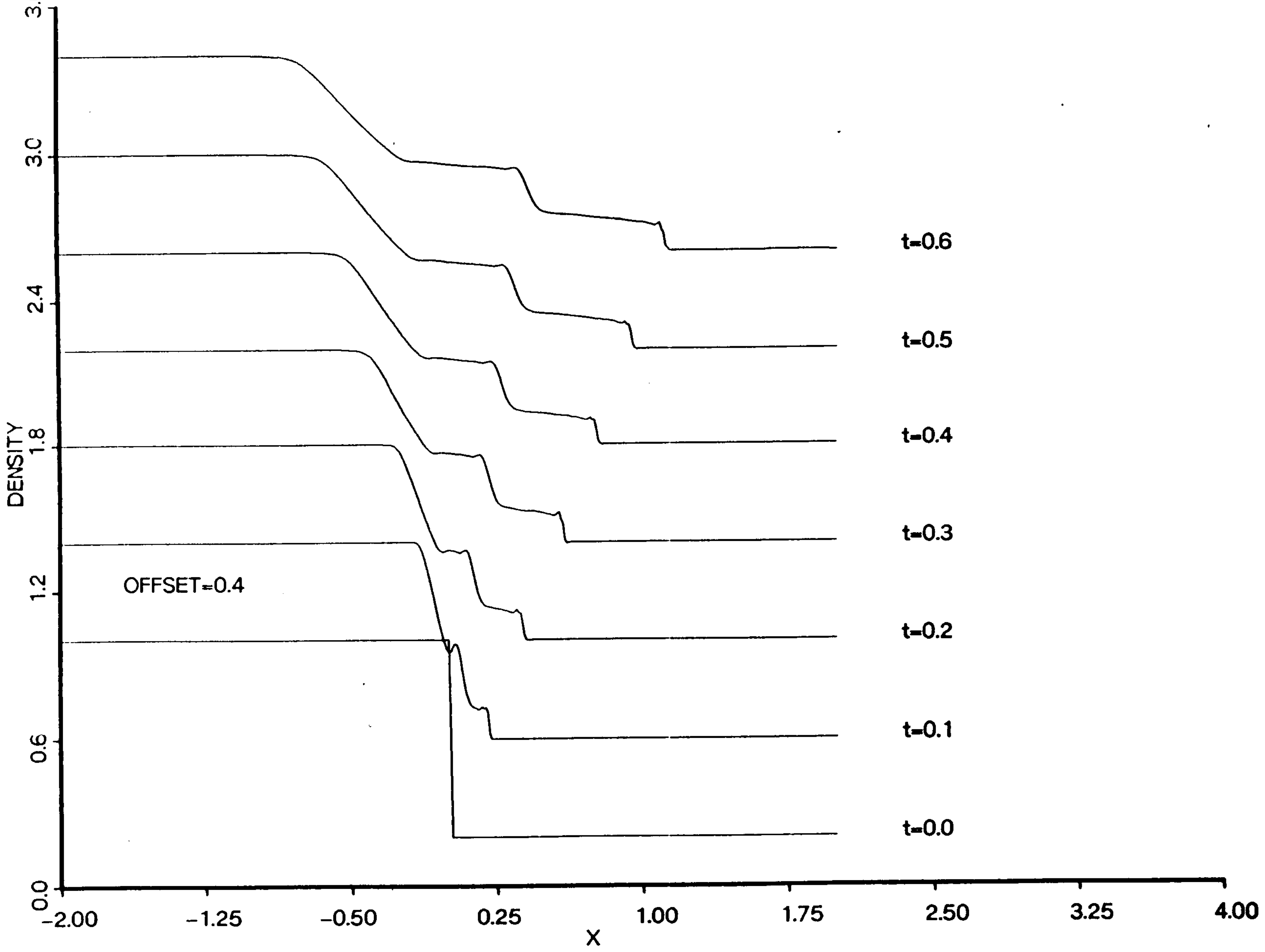
3.6
3.0
2.4
1.8
1.2
0.6
0.0
DENSITY
−2.00
−1.25
−0.50
0.25
1.00
1.75
2.50
3.25
4.00
X
OFFSET=0.4
t=0.6
t=0.5
t=0.4
t=0.3
t=0.2
t=0.1
t=0.0

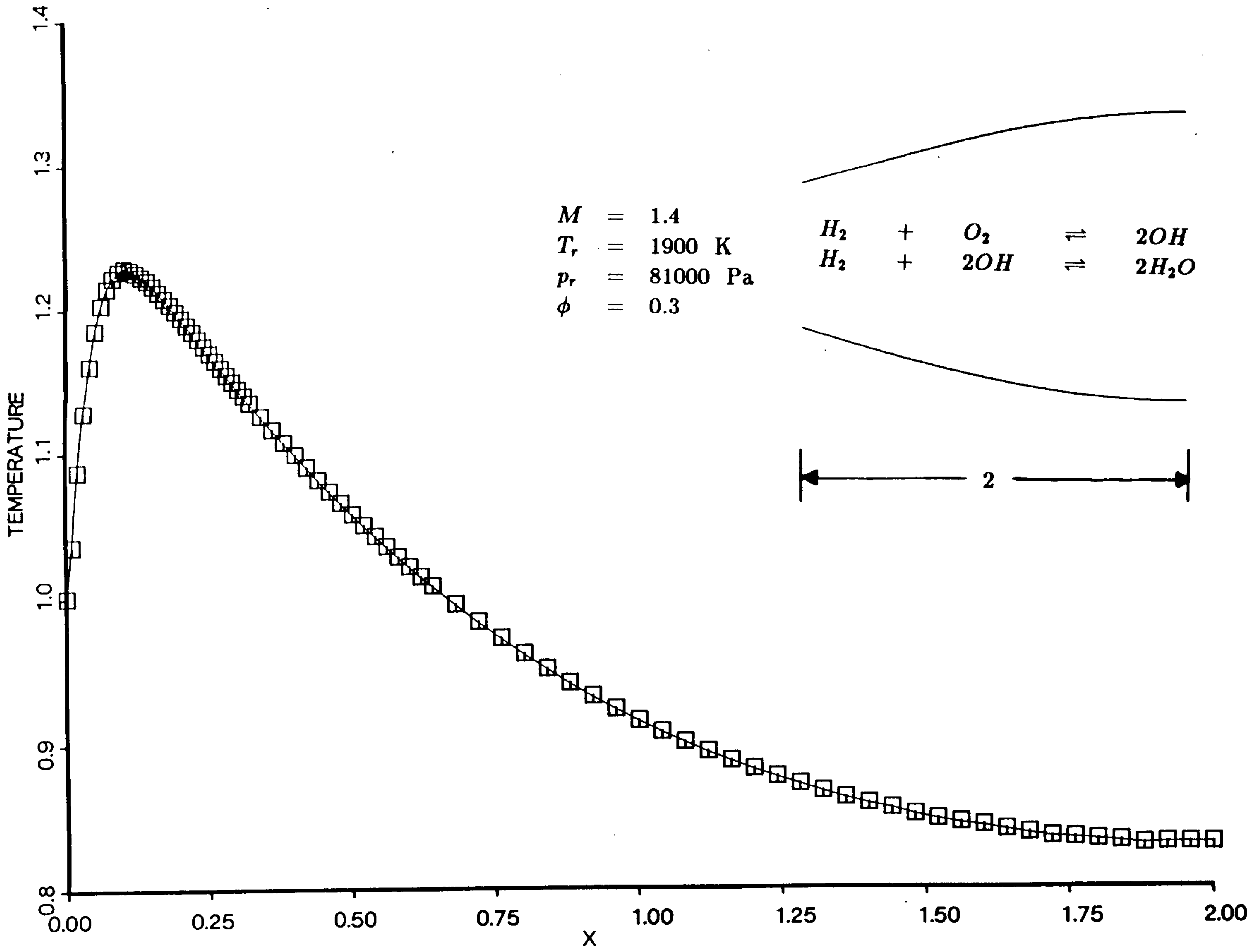
TEMPERATURE
1.4
1.3
1.2
1.1
1.0
0.9
0.8
X
0.00
0.25
0.50
0.75
1.00
1.25
1.50
1.75
2.00
$M = 1.4$
$T_r = 1900$ K
$p_r = 81000$ Pa
$\phi = 0.3$
$H_2 + O_2 \rightleftharpoons 2OH$
$H_2 + 2OH \rightleftharpoons 2H_2O$
2

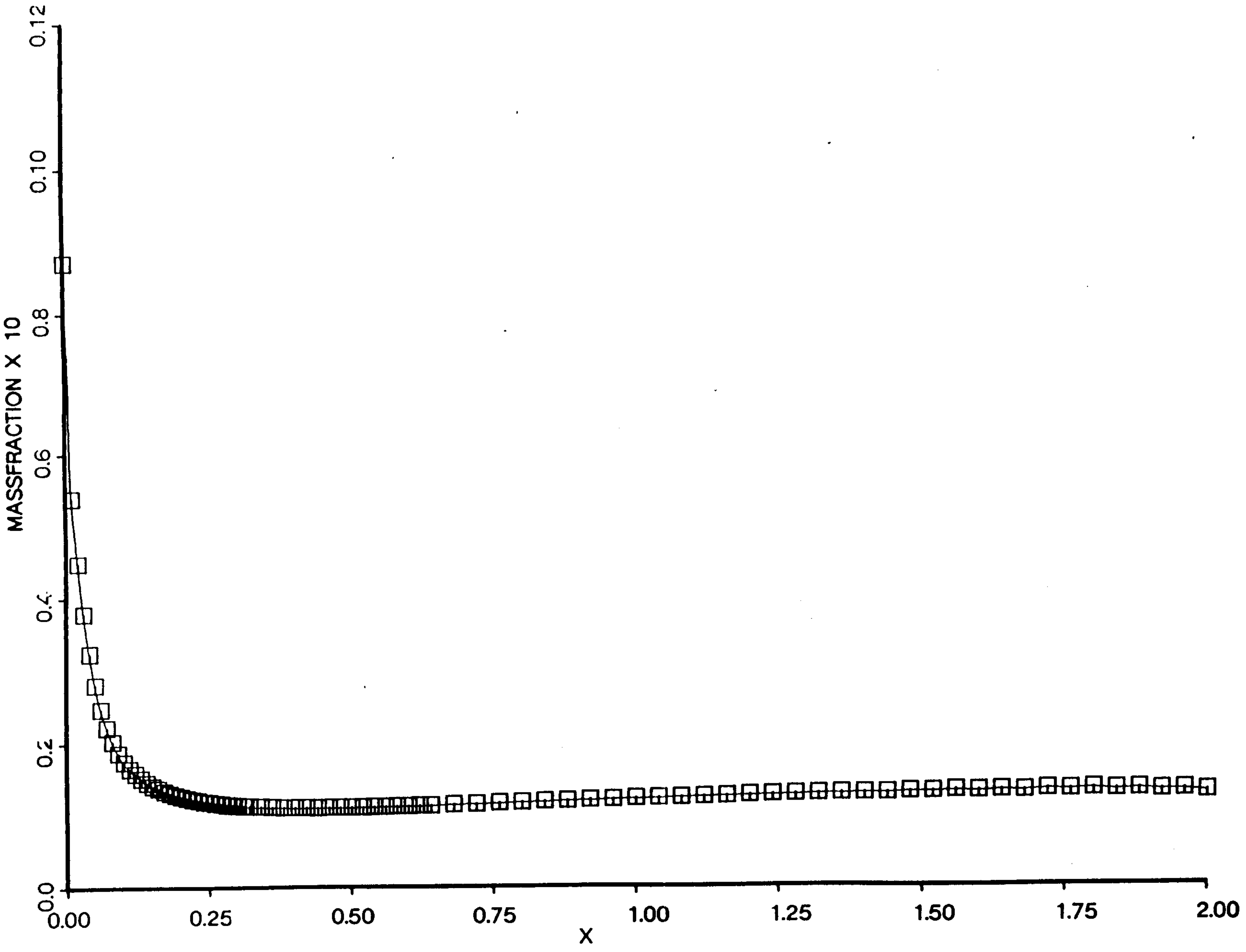
MASSFRACTION X 10 2
0.0
0.2
0.4
0.6
0.8
0.10
0.12
0.00
0.25
0.50
0.75
1.00
1.25
1.50
1.75
2.00
X

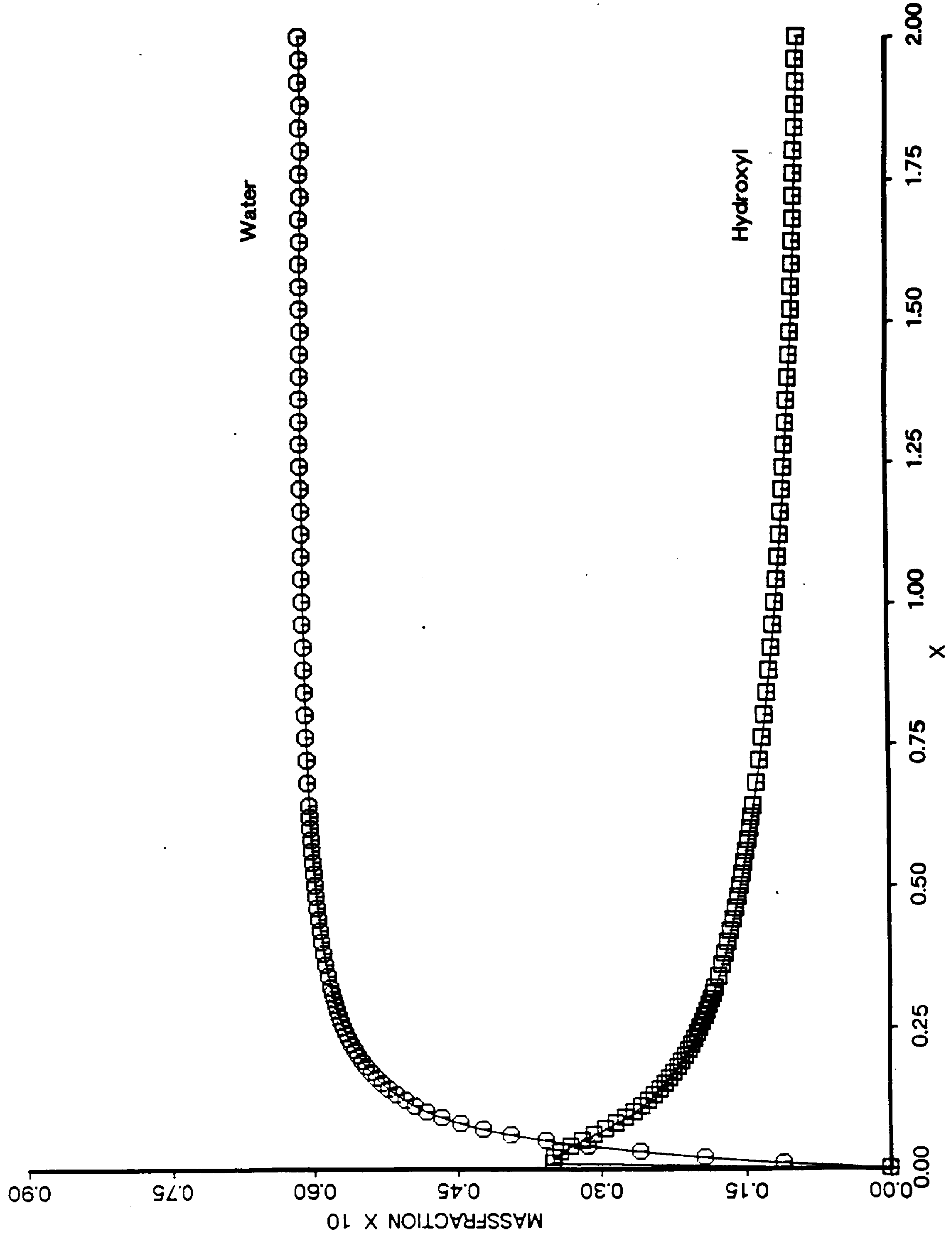
Water
Hydroxyl
MASSFRACTION X 10
0.00
0.15
0.30
0.45
0.60
0.75
0.90
X
0.00
0.25
0.50
0.75
1.00
1.25
1.50
1.75
2.00